Research Article

Journal of Environmental Nanotechnology

Influence of Precursor Molar Concentration on the Morphology and Electrochemical Performance of Tin oxide Nanoparticles

A. Priyadharsini[1*], M. Saravanakumar[2], R. Banupriya[2] and K. Kalaiselvi[3]

[1]Department of Physics, Bannari Amman Institute of Technology, Sathyamangalam, TN, India
[2]Department of Physics, Gobi Arts & Science College, Gobichettipalayam, TN, India
[3]Department of Internet of Things, Vellalar college for women, Erode, TN, India
Received: 13.03.2026 Accepted: 24.03.2026 Published: 30.03.2026
*priyadharsini.arumugam@gmail.com

ABSTRACT

Despite extensive studies on Tin oxide nanoparticles for energy storage applications, the role of precursor molar concentration as a simple and scalable parameter to simultaneously tune morphology, electronic structure, and electrochemical performance remains insufficiently explored. In this work, Tin oxide nanoparticles were synthesized *via* a co-precipitation method using precursor concentrations of 0.3, 0.4, and 0.5 M to systematically investigate this relationship. The results reveal that increasing molar concentration leads to a significant growth in crystallite size from ~5 nm to ~15 nm, accompanied by a reduction in optical band gap from 2.92 eV to 2.70 eV, indicating enhanced defect states and improved charge transport properties. Morphological evolution from relatively smaller particles to agglomerated secondary nanostructures at higher concentrations provides improved interparticle connectivity, which is beneficial for electrochemical applications. Electrochemical analysis demonstrates that all samples exhibit electrical double-layer capacitive behaviour with good reversibility. Notably, the 0.5 M sample delivers a maximum specific capacitance of 131 Fg^{-1} (CV) and 26 Fg^{-1} (GCD), compared to 79 Fg^{-1} and 14 Fg^{-1} for the 0.3 M sample. The enhanced performance is attributed to the combined effect of increased crystallite size, reduced band gap, and favorable morphological features facilitating efficient ion diffusion and electron transport. This study establishes a direct correlation between precursor molar concentration and the resulting physicochemical and electrochemical properties of SnO_2 nanoparticles, demonstrating a simple yet effective strategy for optimizing electrode materials for high-performance supercapacitor applications.

Keywords: SnO_2 nanoparticles; Co-precipitation method; Molar concentration; Supercapacitor.

1. INTRODUCTION

Nanostructured materials have emerged as a central focus in modern materials science due to their size-dependent properties, which differ significantly from their bulk counterparts.(Zhang *et al.* 2009; Wang, 2004; Cao and Wang, 2011) The reduced particle size, tunable morphology, and high surface-to-volume ratio impart unique mechanical, optical, electronic, and electrochemical characteristics, making them highly suitable for advanced technological applications, particularly in energy storage systems. Consequently, tailoring nanoscale features has become a key approach for optimizing material performance in electrochemical devices (Simon and Gogotsi, 2008).

Among various nanomaterials, semiconductor metal oxides have attracted substantial attention owing to their structural stability, tunable electronic properties, and rich defect chemistry. Tin oxide, SnO_2 an n-type semiconductor with a wide band gap of 3.6–3.8 eV, crystallizes in the tetragonal cassiterite structure and exhibits excellent chemical and thermal stability. These characteristics, combined with its environmental compatibility and low cost, make Tin oxide a promising candidate for energy storage and conversion applications (Batzill and Diebold, 2005; Comini *et al.* 2009; Kılıç, Ç. and Zunger, 2002).

A distinguishing feature of Tin oxide is its defect-mediated electronic behaviour. The presence of oxygen vacancies and mixed valence states (Sn^{2+}/Sn^{4+}) introduces donor levels near the conduction band, thereby increasing carrier concentration and electrical conductivity (Chen and Mao, 2007). These defects also serve as active sites for surface redox reactions and facilitate ion adsorption and diffusion at the electrode–electrolyte interface. As a result, the electrochemical performance of SnO_2, particularly in supercapacitors and battery systems, is strongly governed by its defect structure and surface characteristics (Lou *et al.* 2008; Wang and Xia, 2013; Dubal *et al.* 2015; Vandana *et al.* 2021).

To date, a wide range of synthesis techniques including hydrothermal, sol–gel, chemical vapor deposition, and co-precipitation methods have been employed to fabricate SnO_2 nanostructures with

controlled morphology and improved performance. Among these, the co-precipitation method offers distinct advantages such as simplicity, low cost, and scalability, making it attractive for practical applications (Gurlo, 2011). However, despite extensive research, achieving precise control over structural features and defect chemistry through simple synthesis parameters remains a significant challenge.

Previous studies have reported that parameters such as pH, temperature, and calcination conditions influence the crystallinity and morphology of SnO_2nanoparticles. While precursor concentration is known to affect nucleation kinetics and particle growth, most reports have primarily focused on structural or optical characteristics, with limited emphasis on correlating these changes with electrochemical performance (Zhang *et al*. 2016). Furthermore, a comprehensive understanding of how precursor molar concentration governs the interplay between crystallite size, defect density, morphology, and charge storage behaviour is still lacking. This gap limits the rational design of SnO_2 -based electrode materials for high-performance supercapacitors.

In this context, the present work aims to establish a clear structure–property–performance relationship by systematically investigating the effect of precursor molar concentration on SnO_2 nanoparticles synthesized via a co-precipitation route. The precursor concentration is varied (0.3, 0.4, and 0.5 M) while maintaining all other synthesis parameters constant, enabling isolation of its specific influence. The resulting changes in crystallite size, morphology, optical band gap, and electrochemical properties including specific capacitance, charge–discharge behaviour and impedance characteristics are comprehensively evaluated.

It is expected that increasing precursor molar concentration will enhance particle growth and modify defect density, leading to reduced band gap, improved electrical conductivity, and enhanced electrochemical performance. By providing quantitative correlations between synthesis conditions and functional properties, this study offers a simple yet effective strategy for optimizing SnO_2 nanomaterials for next-generation supercapacitor applications.

2. EXPERIMENTAL

Tin oxide nanoparticles were synthesized using the chemical co-precipitation method (Fig. 1). Tin(II) chloride dihydrate ($SnCl_2{\cdot}2H_2O$) was used as the precursor. Initially, a 0.3 M solution of $SnCl_2{\cdot}2H_2O$ (corresponding to 0.3 mol L^{-1} in 50 mL of solution) was prepared by dissolving the required amount in 50 mL of deionized water under constant magnetic stirring at 300 rpm for 30 min. Subsequently, 50 mL of 2-propanol was slowly added to the solution to obtain a total volume of 100 mL. Aqueous ammonia was then added at a controlled rate of ~0.5 mL min^{-1} using a burette as a precipitating agent until the solution reached a final pH of ~9–10. The solution was further stirred continuously for 1 hour to ensure complete precipitation. The resulting mixture was centrifuged and washed once with ethanol and several times with distilled water to remove residual chloride ions. The obtained white precipitate was dried in a hot air oven at 60 °C for 1 hour, followed by additional drying until constant weight was achieved to ensure complete removal of residual solvents. The dried precursor was then calcined in a muffle furnace at 300 °C for 2 hours. Finally, the annealed product was cooled to room temperature and ground using a mortar and pestle to obtain fine SnO_2 nanopowder. The synthesis was repeated for precursor concentrations of 0.4 M and 0.5 M to systematically investigate the effect of molar concentration. The selected concentration range was chosen based on preliminary optimization to ensure complete precipitation while avoiding excessive particle growth and agglomeration, thereby enabling a comparative study of structure–property relationships. The overall yield of SnO_2 nanoparticles was found to be approximately 75–85%, calculated based on the theoretical yield from the precursor.

3. RESULTS AND DISCUSSION

3.1 XRD Analysis

The X-ray diffraction (XRD) patterns (Fig. 2) of SnO_2 nanoparticles synthesized at three different precursor molar concentrations (0.3, 0.4, and 0.5 mol L^{-1}) and annealed at 300 °C are presented in Fig. 1. The diffraction peaks confirm that the prepared SnO_2 powders are crystalline in nature and possess a tetragonal rutile structure, which is in good agreement with the standard JCPDS data card No. 41-1445. The absence of additional peaks indicates that the synthesized samples are phase pure. As the precursor molar concentration increases from 0.3 to 0.5 mol L^{-1}, the intensity of the diffraction peaks increases while the full width at half maximum (FWHM) decreases, indicating improved crystallinity and growth of crystallite size (Cullity and Stock, 2001). The prominent diffraction peaks observed at 2θ values of approximately 26.35°, 33.78°, 37.87°, 51.67°, 54.71°, 57.95°, 61.72°, 64.75°, 65.80°, 71.45°, and 78.67° correspond to the crystal planes (110), (101), (200), (211), (220), (002), (310), (112), (301), (202), and (321) respectively, which are characteristic of SnO_2

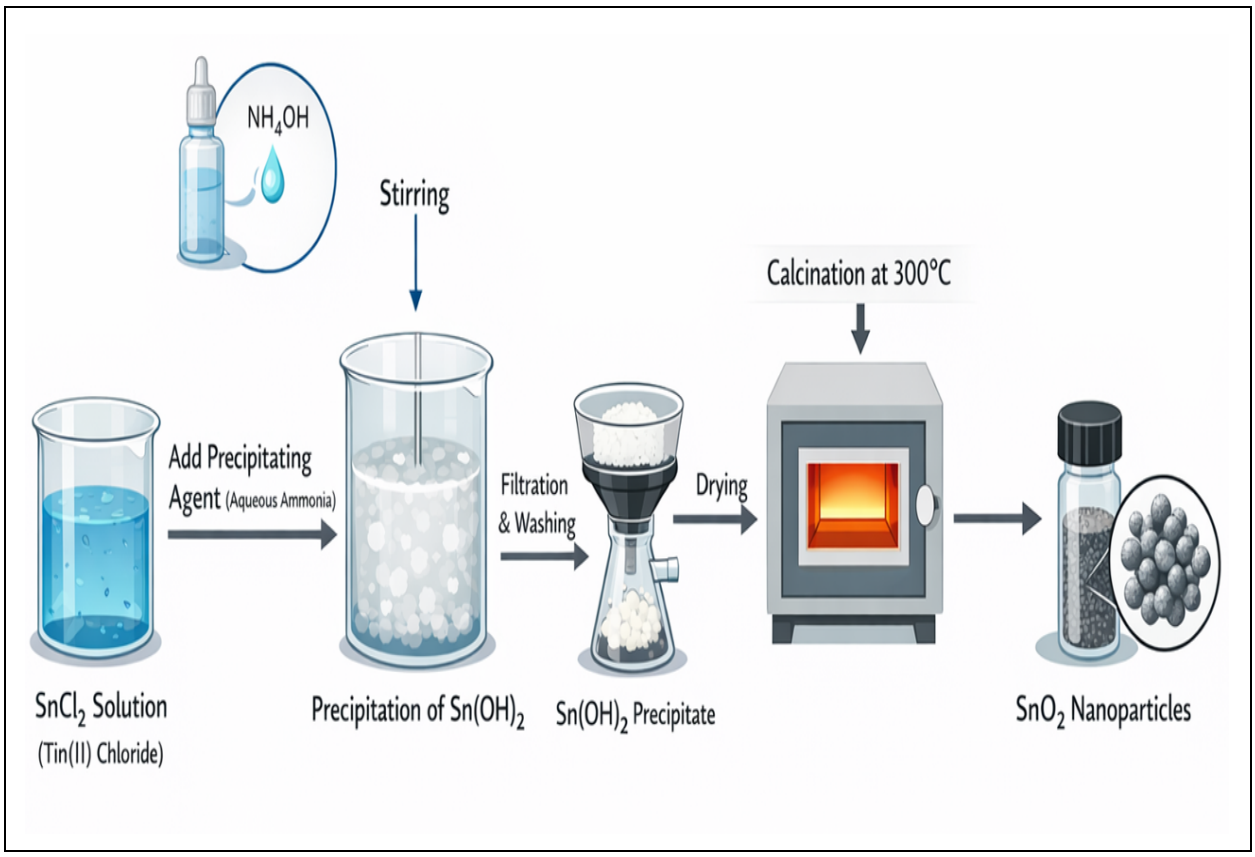


Fig. 1: Preparation of SnO_2 by co-precipitation method

The average crystallite size of the samples was estimated using the Debye–Scherrer equation: (Patterson, 1939)

$$D = k\lambda / \beta \cos\theta \quad \ldots (1),$$

where D represents the crystallite size, k is the shape factor, λ is the wavelength of the X-ray radiation (1.5408 Å), β is the full width at half maximum (FWHM), and θ is the Bragg diffraction angle. The calculated crystallite sizes were found to be approximately 5 nm, 11 nm, and 15 nm for the samples prepared with 0.3, 0.4, and 0.5 mol L^{-1} precursor concentrations, respectively. The increase in crystallite size with precursor concentration can be attributed to enhanced supersaturation during synthesis, which promotes particle growth after nucleation. Larger crystallite size reduces grain boundary resistance, thereby facilitating improved charge transport, which is beneficial for electrochemical performance (Klug and Alexander, 1974).

The microstrain (ε) and dislocation density (δ) were calculated using the relations

$$\varepsilon = \beta\cos\theta/4 \quad \ldots (2)$$

$$\delta = 1/D^2 \quad \ldots (3)$$

The obtained values are in the order of ~10^{14}–10^{16} m^{-2}, which are consistent with reported nanocrystalline oxide materials.

Table 1. Structural parameters using XRD

Molar Concentration	2 θ	Average Grain Size	Strain	Dislocation Density
0.3	26.5770	5 nm	0.00292	1.52213E+19
	33.8434		-0.00142	5.68437E+19
	51.7300		0.003028	1.69789E+19
0.4	26.4463	11nm	0.002872	1.43214E+19
	33.7420		-0.00141	5.46347E+19
	51.6416		0.002949	1.66799E+19
0.5	26.5898	15 nm	0.002542	1.26226E+19
	33.8849		-0.0014	5.30146E+19
	51.8808		0.002801	1.68341E+19

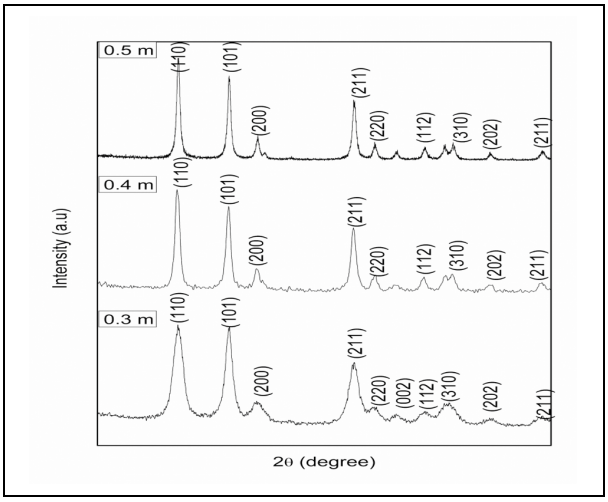


Fig. 2: XRD patterns of pure SnO_2 for three different molar concentrations

3.2 Scanning Electron Microscopy Analysis and EDAX Spectrum

The surface morphology of the synthesized SnO_2 nanoparticles prepared at different precursor molar concentrations and annealed at 300 ℃ (consistent with XRD analysis) was examined using scanning electron microscopy (SEM). The SEM micrographs reveal that the particles exhibit a predominantly agglomerated and particulate morphology for all the samples. Such agglomeration is commonly observed in nanoscale materials due to the high surface energy and strong interparticle interactions (Goldstein *et al.* 2003). With increasing precursor molar concentration, significant morphological evolution is observed. At lower concentration (0.3 M), relatively smaller particles with moderate agglomeration are formed, whereas at higher concentrations (0.5 M), the formation of secondary nanoparticles and larger agglomerated clusters becomes more prominent, as shown in Fig. 3(a), (b), and (c).

This behavior can be explained mechanistically as higher precursor concentration increases supersaturation, leading to rapid nucleation followed by particle growth and collision-induced aggregation. Additionally, the increased particle density enhances van der Waals attractive forces, promoting agglomeration and formation of secondary structures. The observed increase in crystallite size from XRD correlates well with SEM results, confirming that higher molar concentration leads to particle growth and aggregation. These interconnected nanoparticle networks can provide improved electron transport pathways and facilitate electrolyte ion diffusion, thereby enhancing electrochemical performance.

The chemical composition and purity of the synthesized nanoparticles were further analyzed using Energy Dispersive X-ray Analysis (EDAX). The EDAX spectra (Fig. 4) obtained for all three samples prepared at different molar concentrations confirm the presence of only Sn and O elements. No impurity peaks corresponding to other elements were detected, indicating the high purity of the synthesized SnO_2 nanoparticles. In particular, the absence of chlorine peaks confirms that the chloride ions originating from the precursor ($SnCl_2 \cdot 2H_2O$) were completely removed during the washing and calcination processes (Cullity, 1978).

The purity and controlled morphology of SnO_2nanoparticles are crucial factors for electrochemical applications. The presence of agglomerated nanoparticle networks can provide interconnected pathways for electron transport, while the nanoscale dimensions offer a high active surface area for electrochemical reactions. These characteristics are beneficial for applications such as electrode materials in batteries, supercapacitors, and electrochemical sensors, where efficient charge transfer and enhanced surface reactivity are required.

However, it should be noted that EDAX has limited sensitivity toward light elements and trace impurities; therefore, the absence of impurity peaks does not completely rule out their presence at very low concentrations.

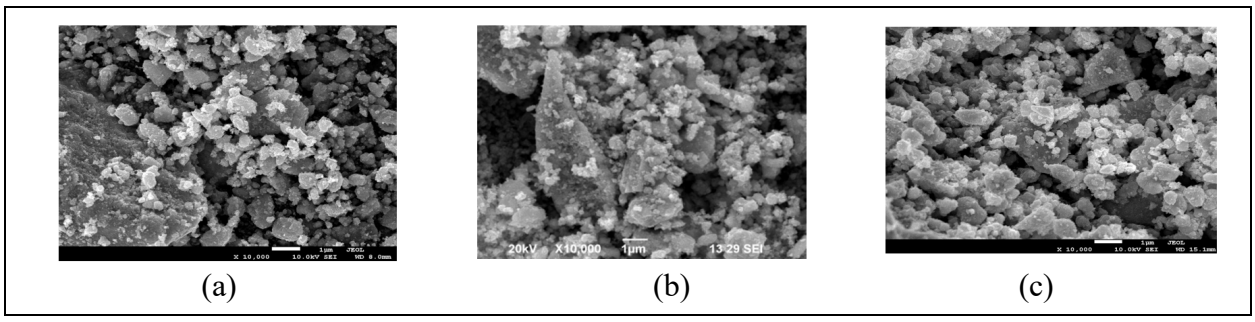


Fig. 3: SEM images of pure SnO_2 nanoparticles (a) 0.3 M (b) 0.4 M and (c) 0.5 M

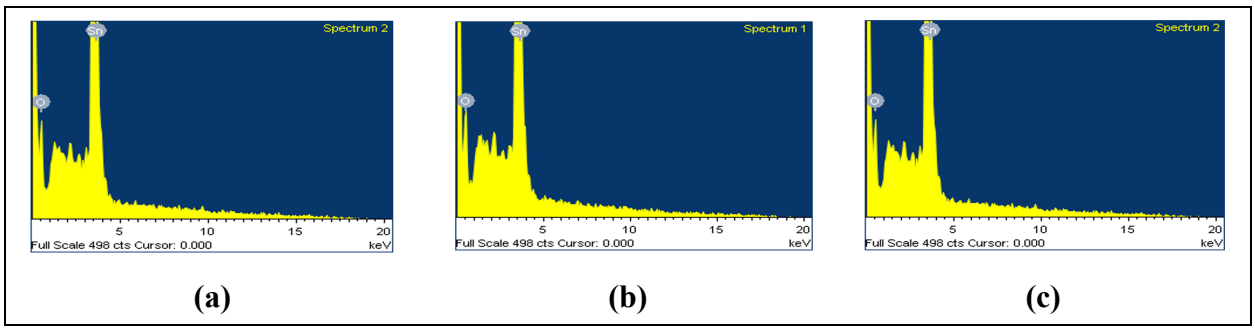


Fig. 4: EDAX spectrum of pure SnO_2 nanoparticles (a) 0.3 M (b) 0.4 M and (c) 0.5 M

3.3 UV Studies

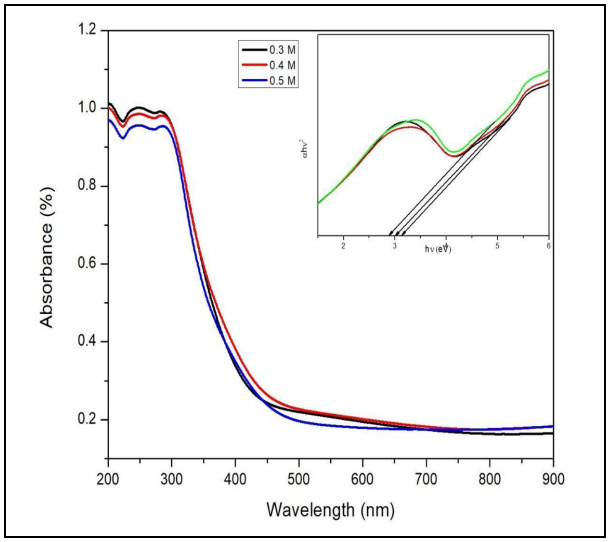


Fig. 5: UV spectra of pure SnO_2 nanoparticles (a) 0.3 m (b) 0.4 m and (c) 0.5 m inset shows the Tauc's plot

The UV–visible absorption spectra (Fig. 5) of the SnO_2 nanoparticles synthesized at different precursor molar concentrations were recorded using a UV–visible spectrophotometer (e.g., Shimadzu UV-2600) in the wavelength range 200–800 nm, with baseline correction performed using a blank solvent reference to study their optical properties.

The optical band gap energies of the samples were estimated using the Tauc relation: (Tauc, 1968)

$$\alpha h\nu = A\,(h\nu - Eg)^n \qquad \ldots (4)$$

where α is the absorption coefficient, hν represents the photon energy, E_g is the optical band gap energy, A is a constant, and n indicates the nature of the electronic transition. For SnO_2which is widely reported as a direct band gap semiconductor, the value of n = 1/2 is used for direct allowed transitions (Davis and Mott, 1970). Accordingly, the plots of $(\alpha h\nu)^2$ versus photon energy (hν) were constructed, and the band gap values were determined by extrapolating the linear portion of the plot to intersect the photon energy axis at $(\alpha h\nu)^2 = 0$. The results indicate that the optical band gap of SnO_2nanoparticles decreases with increasing precursor molar concentration. This red shift in absorption edge can be attributed to the combined effect of increased crystallite size and the introduction of defect states, particularly oxygen vacancies, which create localized energy levels within the band gap. These defect states facilitate sub-bandgap optical transitions and effectively reduce the observed band gap energy. Furthermore, the obtained band gap values are slightly lower than the bulk SnO_2 band gap, which may be associated with defect-induced band tailing (Urbach energy) and increased structural disorder at higher precursor concentrations. The increase in precursor concentration enhances supersaturation during synthesis, leading to higher defect density and oxygen vacancy formation, which in turn modifies the electronic structure of SnO_2. The variation in band gap with precursor molar concentration suggests that the optical and electronic properties of SnO_2 nanoparticles can be effectively tuned through synthesis conditions. This reduction in band gap is beneficial for electrochemical applications, as it enhances electrical conductivity and facilitates faster charge transfer processes at the electrode–electrolyte interface. The calculated band gap values for the three different concentrations are summarized in Table 2.

Table 2. Bandgap energy values for three molar concentrations

S. No.	Molar Concentration	Bandgap Energy in eV
1.	0.3 M	2.920
2.	0.4 M	2.880
3.	0.5 M	2.702

3.4 FTIR

Fourier Transform Infrared (FTIR) spectroscopy was employed to identify the functional groups and analyze the chemical bonding present in the synthesized SnO_2 nanoparticles. The FTIR spectra (Fig. 6) were recorded in the range 4000–400 cm^{-1} to obtain a comprehensive understanding of the vibrational modes. The spectrum exhibits a prominent peak at around 611.58

cm^{-1} which is attributed to the O–Sn–O antisymmetric stretching vibration, confirming the formation of the SnO_2lattice structure. (Wang *et al*. 2012) Another band observed near 566 cm^{-1} corresponds to the Sn–O stretching or terminal Sn–OH vibration modes. These bands are in good agreement with reported FTIR signatures of SnO_2 nanoparticles in the literature, typically observed in the range 500–700 cm^{-1}. In addition to these characteristic peaks, broad peaks observed in the region 3200–3500 cm^{-1} are assigned to the stretching vibrations of hydroxyl (–OH) groups, while the peak around ~1620 cm^{-1} corresponds to the bending mode of adsorbed water molecules. (Nakamoto, 2009; Socrates, 2004) These features indicate the presence of surface-adsorbed moisture, which is commonly observed in oxide nanomaterials due to their high surface area. Weak peaks in the region 1000–1400 cm^{-1} may be attributed to residual organic species or carbonate groups formed due to atmospheric CO_2 adsorption during sample handling. The presence of these minor bands does not affect the overall phase formation but reflects surface interactions typical of nanoscale oxides.

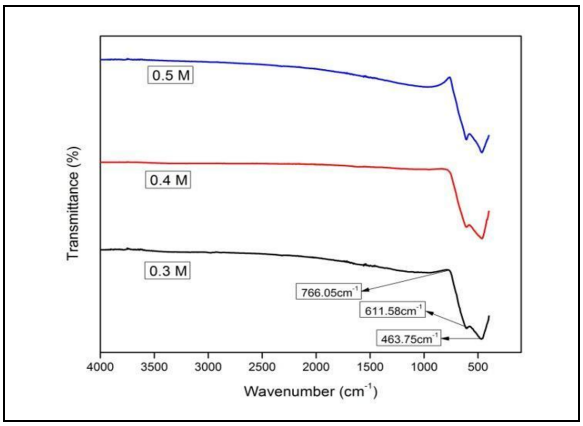


Fig. 6: FTIR spectra for 0.3, 0.4, 0.5 M concentrations

3.5 Electrochemical Behavior

The electrode materials play a crucial role in determining the performance of supercapacitors. Therefore, significant research efforts have been directed toward improving electrode materials to enhance energy storage performance (Conway, 1999). In this context, various carbon-based materials such as activated carbon, graphene, and mesoporous carbon have been widely explored as electrode materials or conductive supports for transition metal oxides. These materials provide high surface area, good electrical conductivity, and enhanced electrochemical stability, which contribute to improved charge storage characteristics (Miller and Simon, 2008). In particular, graphene-based systems have attracted considerable attention due to their excellent electrical conductivity and large surface area, making them promising for advanced energy storage applications such as electric vehicles, renewable energy systems, and smart grids.

3.5.1 Cyclic Voltammetry

The electrochemical behaviour of the synthesized SnO_2 nanoparticles was investigated using cyclic voltammetry (CV). The obtained CV curves exhibit a quasi-rectangular shape, indicating good reversibility and predominant electrical double layer capacitance (EDLC) behaviour of the electrode material (Bard and Faulkner, 2011; Trasatti and Buzzanca, 1971). In EDLC-based systems, charge storage occurs through the accumulation of electrolyte ions at the electrode–electrolyte interface, enabling rapid charge–discharge processes and good cycling stability.

The specific capacitance of the electrode material was calculated using the following relation: (Zhang and Zhao, 2009)

$$C = \frac{1}{mv(V_C - V_A)} \int_{V_C}^{V_A} I(V)dv \qquad Fg^{-1} \ldots (5),$$

Where C is the Specific capacitance, $(V_C - V_A)$is potential window, m is the mass of the active material, v is the scan rate (mV/S) and $\int_{V_C}^{V_A} I(V)dv$ represents the total voltametric charge obtained by integration of positive and negative sweep in cyclic voltammograms. The specific capacitance of pure SnO_2 electrodes at various scan rates is shown in Fig. 7. The value of specific capacitance decreases with increase in scan rate from 5mV/S to 100mV/S. The decrease in specific capacitance with scan rate is obviously due to the inadequate time accessible for diffusion and adsorption in the interior of smallest pores at high scan rates (Barsoukov and Macdonald, 2005). The capacitance values were found to be 79 Fg^{-1} 121 Fg^{-1} and 131 Fg^{-1} for 0.3 M, 0.4 M, and 0.5 M samples, respectively. The increase in capacitance with precursor molar concentration can be correlated with structural and morphological evolution. As observed from XRD, the increase in crystallite size reduces grain boundary resistance, thereby improving electrical conductivity (Frackowiak and Beguin, 2001). The SEM analysis reveals the formation of interconnected agglomerated nanoparticle networks at higher concentrations, which provide continuous pathways for electron transport and facilitate electrolyte ion diffusion.

In addition, the reduction in optical band gap observed from UV–visible analysis indicates enhanced electronic conductivity, which further contributes to improved electrochemical performance. Thus, the combined effect of improved crystallinity, particle connectivity, and electronic structure leads to enhanced capacitance for the 0.5 M sample.

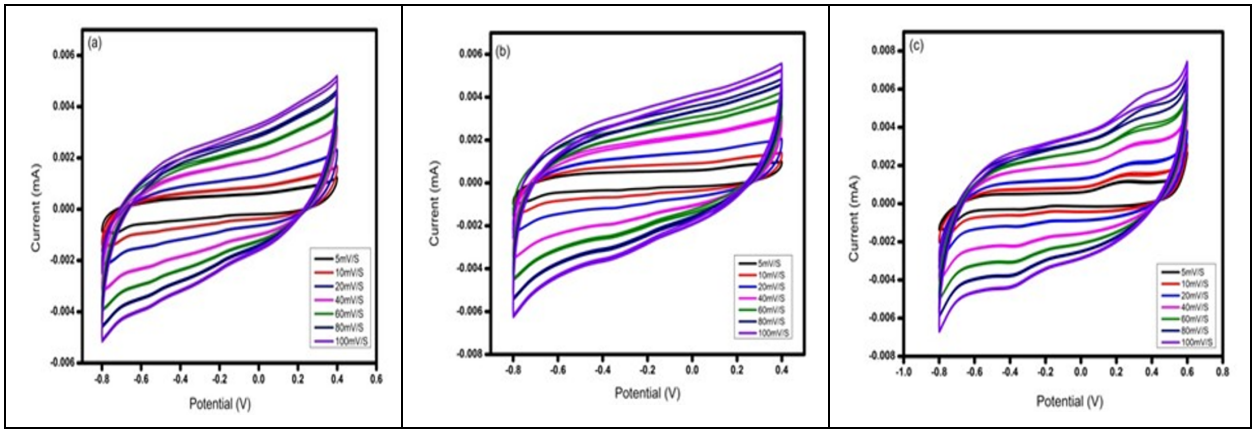


Fig. 7: CV graphs of 0.3, 0.4, 0.5 M concentrations

3.5.2 Galvanostatic Charge-discharge Analysis

The galvanostatic charge and discharge analysis of SnO_2 nanoparticles annealed at 300 °C for three different molar concentrations of tin source as 0.3 M, 0.4M and 0.5 M in the potential window is shown in the Fig. 8. This is an imposing analysis for estimating the electrochemical performance of electrode materials with constrained current rates. The galvanostatic charge discharge analysis with graphene electrode was done in the potential window range -0.8 to 0.4 V at various current densities such as 0.5 to 5 A/g for 2 M KOH concentration. The specific capacitance values were found from the formula (Winter and Brodd, 2004)

$$C = \frac{I\,\Delta t}{m\,\Delta V}\ \mathrm{Fg^{-1}} \qquad \ldots (6)$$

Where I/m stands for current density, Δt is discharging time and ΔV is potential window.

The specific capacitance values obtained from galvanostatic charge discharge studies are 14, 17 and 26 F/g for the samples prepared for 0.3, 0.4, 0.5 molar concentrations at 300 °C Although these values are lower compared to those obtained from CV analysis, such variation is commonly observed due to differences in measurement techniques (Liu *et al*. 2010). The relatively lower capacitance values can be attributed to factors such as particle agglomeration, reduced effective surface area, and limited electrolyte penetration into the inner regions of the electrode material (Liu *et al.* 2015).

However, the gradual increase in capacitance with increasing precursor concentration suggests improved charge transport and enhanced interaction between the electrode and electrolyte. This trend is consistent with the structural and morphological observations, confirming that higher precursor concentration promotes better electrochemical performance.

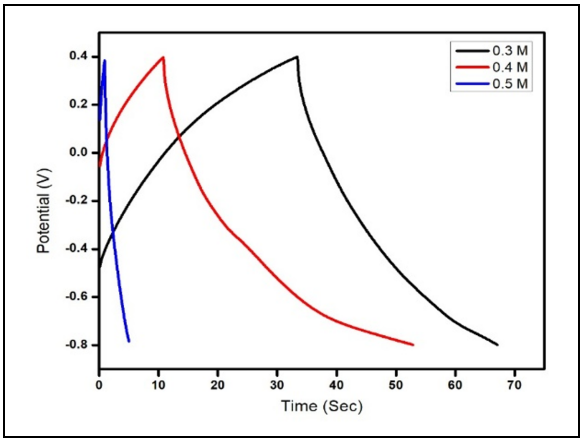


Fig. 8: GCD graphs of 0.3, 0.4, 0.5 M concentrations

3.7.3 Electrochemical Impedance Spectroscopy

Electrochemical impedance spectroscopy (EIS) measurements were carried out in the frequency range 0.001 Hz to 100 kHz with an AC amplitude of 5 mV (Fig. 9). The Nyquist plots typically consist of a semi-circular region in the high-frequency range followed by a straight line in the low-frequency region (Gautam *et al.* 2025). The high-frequency semicircle corresponds to the solution resistance (R_s) and charge transfer resistance (R_{ct}), while the straight line at low frequencies represents the capacitive behaviour and ion diffusion characteristics of the electrode material. The nearly vertical nature of the low-frequency line indicates good capacitive behaviour and efficient ion diffusion at the electrode–electrolyte interface. With increasing precursor molar concentration, a reduction in the diameter of the semicircle is observed, indicating decreased charge transfer resistance and improved electrical conductivity (Ramesh *et al*. 2019). This enhancement can be attributed to improved crystallinity, reduced grain boundary resistance, and better particle connectivity, as confirmed by XRD and SEM analyses.

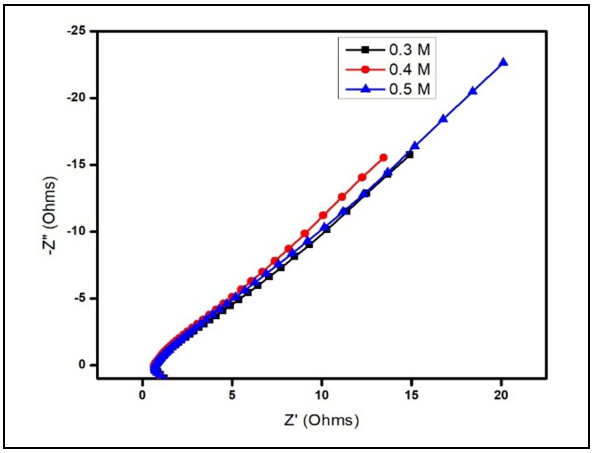


Fig. 9: Nyquist plots for SnO_2 made using three molar concentrations

4. CONCLUSION

In this work, SnO_2 nanoparticles were synthesized *via* a simple, cost-effective co-precipitation method with varying precursor molar concentrations. Increasing concentration enhanced crystallinity and crystallite size (5–15 nm) while maintaining a tetragonal rutile structure with high purity. The SEM studies showed agglomerated particles, and EDAX confirmed only Sn and O elements. The band gap slightly decreased with higher concentration, likely due to larger crystallites and oxygen vacancies. Infrared spectroscopy verified Sn–O bonding. Electrochemical studies revealed good capacitive behavior, with quasi-rectangular CV curves indicating electrical double-layer capacitance. The 0.5 M sample exhibited the highest specific capacitance and improved charge transfer, highlighting SnO_2 nanoparticles as promising materials for supercapacitor applications.

FUNDING

This research received no specific grant from any funding agency in the public, commercial, or not-for-profit sectors.

CONFLICTS OF INTEREST

The authors declare that there is no conflict of interest.

COPYRIGHT

This article is an open-access article distributed under the terms and conditions of the Creative Commons Attribution (CC BY) license (http://creativecommons.org/licenses/by/4.0/).

REFERENCES

Bard, A. J. and Faulkner, L. R., Electrochemical methods: Fundamentals and applications, 2nd Ed., *Wiley, New York*, 864(2011).

Barsoukov, E. and Macdonald, J. R., Impedance spectroscopy: Theory, experiment, and applications, *Wiley, New Jersey,* 517-528(2005).

Batzill, M. and Diebold, U., The surface and materials science of tin oxide, *Prog. Surf. Sci.*, 79(2–4), 47–154 (2005). https://doi.org/10.1016/j.progsurf.2005.09.002

Cao G. and Wang Y., Nanostructures and nanomaterials: Synthesis, properties and applications, *World Scientific*, 596(2011). https://doi.org/10.1142/7885

Chen, X. and Mao, S. S., Titanium dioxide nanomaterials: Synthesis, properties, modifications, and applications, *Chem. Rev.*, 107(7), 2891–2959 (2007). https://doi.org/10.1021/cr0500535

Comini, E., Faglia G., Sberveglieri G., Baratto, C., Ferroni, M. and Vomiero, A., Quasi-one-dimensional metal oxide semiconductors: Preparation, characterization and application as chemical sensors, *Prog. Mater. Sci.*, 54(1), 1–67 (2009). https://doi.org/10.1016/j.pmatsci.2008.06.003

Conway, B. E., Electrochemical supercapacitors: Scientific fundamentals and technological applications, *Springer, New York*, 698(1999). https://doi.org/10.1007/978-1-4757-3058-6

Cullity, B. D. and Stock, S. R., Elements of X-ray diffraction, 3rd Ed., Prentice Hall, New Jersey (2001).

Cullity, B. D., Elements of X-ray diffraction, *Addison-Wesley, Massachusetts,* 95(1978).

Davis, E. A. and Mott, N. F., Conduction in non-crystalline systems, *Philos. Mag.*, 22(179), 903–922 (1970). https://doi.org/10.1080/14786437008221061

Dubal, D. P., Ayyad, O., Ruiz, V. and Gómez-Romero, P., Hybrid energy storage: The merging of battery and supercapacitor chemistries, *Chem. Soc. Rev.*, 44(7), 1777–1790 (2015). https://doi.org/10.1039/C4CS00266K

Frackowiak, E. abd Béguin F., Carbon materials for electrochemical energy storage of energy in capacitors, *Carbon*, 39(6), 937–950 (2001). https://doi.org/10.1016/S0008-6223(00)00183-4

Gautam, N. K., Sharma, A., Varshney, M., Singh, J. P., Shin, H. J., Kumar, S., Brajpuriya, R., Lee, B., Chae, K. H. and Won S. O., SnO_2/Na–SnO_2@MXene hybrid electrode materials for supercapacitor applications, *New J. Chem.*, 49, 11203–11217 (2025). https://doi.org/10.1039/D5NJ00196J

Goldstein, J. I., Newbury, D. E., Joy, D. C., Lyman, C. E., Lifshin, E., Sawyer L., Michael J.R., Scanning electron microscopy and X-ray microanalysis, *Springer New York*, 550(2003).

Gurlo A., Nanosensors: Towards morphological control of gas sensing activity, *Nanoscale*, 3(1), 154–165 (2011). https://doi.org/10.1039/C0NR00441C

Kılıç, Ç. and Zunger, A., Origins of coexistence of conductivity and transparency in SnO_2, *Phys. Rev. Lett.*, 88(9), 095501 (2002). https://doi.org/10.1103/PhysRevLett.88.095501

Klug H. P. and Alexander L. E., X-ray diffraction procedures for polycrystalline materials, *Wiley,* (1974).

Liu, C., Li, F., Ma, L. P. and Cheng, H. M., Advanced materials for energy storage, *Adv. Mater.*, 22(8), E28–E62 (2010). https://doi.org/10.1002/adma.200903328

Liu, L., An, M., Yang, P. and Zhang, J., Superior cycle performance and high reversible capacity of SnO_2/graphene composite as an anode material, *Sci. Rep.*, 5, 9055 (2015). https://doi.org/10.1038/srep09055

Lou, X. W., Archer, L. A. and Yang Z., Hollow micro/nanostructures: Synthesis and applications, *Adv. Mater.*, 20(21), 3987–4019 (2008). https://doi.org/10.1002/adma.200800854

Miller, J. R. and Simon, P., Electrochemical capacitors for energy management, *Sci.*, 321(5889), 651–652 (2008). https://doi.org/10.1126/science.1158736

Nakamoto, K., Infrared and Raman spectra of inorganic and coordination compounds, *Wiley, New York,* 415-419(2009).

Patterson, A. L., The Scherrer formula for X-ray particle size determination, *Phys. Rev.*, 56(10), 978–982 (1939). https://doi.org/10.1103/PhysRev.56.978

Ramesh, S., Yadav, H. M., Lee, Y. J., Hong, G. W., Kathalingam, A., Sivasamy, A., Kim, H. S., Kim, H. S. and Kim, J. H., Porous nitrogen-doped graphene oxide/SnO_2 composite for supercapacitor applications, *Sci. Rep.*, 9, 12622 (2019). https://doi.org/10.1038/s41598-019-48951-2

Simon P. and Gogotsi Y., Materials for electrochemical capacitors, *Nat. Mater.*, 7(11), 845–854 (2008). https://doi.org/10.1038/nmat2297

Socrates G., Infrared and Raman characteristic group frequencies, *Sci.*, 368(2004).

Tauc, J., Optical properties and electronic structure of amorphous semiconductors, *Mater. Res. Bull.*, 3(1), 37–46 (1968). https://doi.org/10.1016/0025-5408(68)90023-8

Trasatti, S. and Buzzanca. G., Ruthenium dioxide: A new interesting electrode material, *J. Electroanal. Chem. Interf. Electrochem.*, 29(2), A1–A5 (1971). https://doi.org/10.1016/S0022-0728(71)80111-0

Vandana, M., Nagaraju, Y. S., Ganesh, H., Veeresh S., Vijeth H., Basappa, M. and Devendrappa, H., A SnO_2 quantum dots/GO/PPY ternary composite film as positive electrode for solid-state asymmetric supercapacitor, *RSC Adv.*, 11, 27801–27811 (2021). https://doi.org/10.1039/D1RA03423E

Wang, W., Hao, Q., Lei, W., Xia, X. and Wang, X., Graphene/SnO_2/polypyrrole ternary nanocomposites as supercapacitor electrode materials, *RSC Adv.*, 2, 10268–10274 (2012). https://doi.org/10.1039/C2RA21292G

Wang, Y. and Xia, Y., Recent progress in supercapacitors: From materials design to system construction, *Adv. Mater.*, 25(37), 5336–5342 (2013). https://doi.org/10.1002/adma.201301532

Wang, Z. L., Zinc oxide nanostructures: Growth, properties and applications, *J. Phys.: Condens. Matter*, 16(25), R829–R858 (2004). https://doi.org/10.1088/0953-8984/16/25/R01

Winter, M. and Brodd, R. J., What are batteries, fuel cells, and supercapacitors?, *Chem. Rev.*, 104(10), 4245–4269 (2004). https://doi.org/10.1021/cr020730k

Zhang, H., Chen, G. and Bahnemann, D.W., Visible-light photocatalytic materials: From synthesis to applications, *J. Mater. Chem.*, 19(28), 5089–5121 (2009). https://doi.org/10.1039/B821991E

Zhang, J., Liu, X., Neri, G. and Pinna N., Nanostructured materials for room-temperature gas sensors, *Adv. Mater.*, 28(5), 795–831 (2016). https://doi.org/10.1002/adma.201503825

Zhang, L. L. and Zhao, X. S., Carbon-based materials for supercapacitors, *Chem. Soc. Rev.*, 38(9), 2520–2531 (2009). https://doi.org/10.1039/B813846J